STUDY OF THE WEAR RESISTANCE PLASMA NITRIDED GGG60 BY OPTIMIZATION OF SURFACE TREATMENT CONDITIONS USING RESPONSE SURFACE METHODOLOGY

İsmail Aykut Karamanli
Department of Sorgun Vocational School, Yozgat Bozok University, Yozgat, Turkey

Mustafa Sabri Gök and Yılmaz Küçük
Department of Mechanical Engineering, Bartın University, Bartın, Turkey

Okan Ünal
Department of Mechanical Engineering, Karabük University, Karabük, Turkey

Copyright © 2024 The Author(s)
https://doi.org/10.1007/s40962-024-01310-y

Abstract

In this study, the wear performance of spheroidal graphite cast iron subjected to plasma nitriding at different temperatures and treatment durations was investigated. The plasma nitriding parameters were optimized by response surface methodology (RSM) due to the output performance. Plasma nitriding was applied at three different temperatures (400, 450, 500 °C) and three different heat treatment durations (0.5, 2, 4 h). Wear tests were performed by ball-on-disk method for 60 minutes and for three different wear loads (10, 20, 30 N). The specimens were investigated for hardness, microstructure and wear performance. The RSM model was then created by using the wear resistance features. Plasma nitriding showed better wear performance than the untreated specimen for all treatment conditions. Hardness, nitrided layer thickness and wear performance remarkably improved with increasing temperature and process duration. The parameter that affects volume loss the most is wear load with 70.66% according to RSM modeling results. The most effective parameter in the wear rate change was found to be treatment duration at 42.85%. The model was able to predict the results with an error of 2.11% for volume loss and 9.14% for wear rate. The prediction results are very close to the experimental results. This clearly shows that the model can be used to determine the plasma nitriding parameters.

Keywords: *spheroidal graphite cast iron, plasma nitriding, wear rate, tribology, optimization, response surface methodology, RSM*

Introduction

Spheroidal graphite (SG) cast iron, in other words ductile iron is a widely used material in various industrial applications due to its excellent mechanical properties and low production cost.[1,2] SG cast iron is well differentiated from other cast materials by having good mechanical strength, high toughness, high fatigue and wear resistance, excellent castability and low specific weight.[1,3,4] These properties make SG cast iron suitable for use in gears, camshafts, crankshafts, machine guides and cast gears.[1,5,6] The fact that tools and components made of this material are frequently subjected to wear and it is important to investigate their wear performance.[7] The wear performance of SG cast iron and the main reasons affecting it have been investigated in many studies. In one study, researchers focused on improving the cutting performance of cermet tools on SG cast iron by adding high entropy carbide. The researchers found that the addition of high entropy carbide improved the cutting performance of tools on SG cast iron.[8] Another study evaluated the effect of heat treatment on the microstructure and wear behavior of a joint manufactured by SG cast iron. The wear behavior of parts produced from SG cast iron was investigated. It was found that the wear behavior of tungsten inert gas (TIG) welded parts were

Received: 28 December 2023 / Accepted: 04 March 2024 /
Published online: 29 March 2024

affected by the preheating applied before welding and the heat affected zone formed during welding. In these zones, graphite nodules were melted due to the high temperature effect and changes in microstructure occurred, which affected the wear performance.[7]

The microstructure is one of the parameters that significantly affect the wear performance of SG cast iron. Surface modification processes can change the microstructure and tribological properties of the surface and subsurface layers.[9] The carbides in spheroidal graphite cast iron can also affect the wear resistance. The effect of carbides on the wear resistance of spheroidal graphite cast iron has been studied. The researchers compared the abrasive wear resistance of different types of SG cast iron and found that the presence of certain carbides increased the wear resistance.[10]

One of the most important factors affecting the properties of spheroidal graphite cast iron is heat treatment. Heat treatment includes subjecting the material to heating and cooling processes under certain ambient conditions to improve its mechanical properties by changing the microstructure in SG cast iron.[11] With heat treatments such as austempering, induction hardening, the microstructure is heated to austenite transformation temperature. Then it is cooled at certain speeds and phase transformations are formed.[11,12] The effects of alloying elements on the behavior of SG cast iron during heat treatment have also been studied. Researchers have shown that the addition of alloying elements such as chromium and molybdenum can affect the hardness of high chromium cast irons and the amount of residual austenite present in the structure. The amount of residual austenite and alloying elements affects the hardness of the material.[13–15] In addition to heat treatment, annealing and tempering can further modify the microstructure and properties of SG cast iron.[13]

Another heat treatment method used to improve the mechanical properties of spheroidal graphite cast iron is nitriding.[6,16,17] The formed compound layers and diffusion zones increase the surface hardness, increase wear resistance and provide improvements in tribological properties.[6,18] However, the negative aspects of classical gas nitriding methods are the long process duration and limited depth of effect. In order to reduce these negative effects, more effective nitriding methods such as nitro-carburizing, plasma nitriding (PN) have been developed.[19,20] Researchers have shown that PN can lead to the formation of a compound layer of iron nitrides, which significantly increases the surface hardness.[19] The thickness and composition of the compound layer formed as a result of PN can be controlled by adjusting process parameters such as temperature and process duration. Thus, the mechanical properties of nitrided materials can be easily changed according to the conditions of use.[19,21] Furthermore, PN is more efficient than gas nitriding in terms of obtaining a deeper diffusion zone and a thicker compound layer.[19] Surface hardness is one of the most effective parameters in wear performance. Similar surface hardness values can be achieved with PN up to 4 times shorter than conventional gas nitriding.[21,22] Thus, time is saved and production times are reduced. With all these advantages, PN becomes an effective surface hardening method by nitriding. PN parameters can affect wear performance. It was found that a hard structure formed on the surface of SG cast iron treated with active screen plasma nitriding (ASPN) consisting of nitride compounds. A diffusion zone was formed under this layer. The thickness and hardness of the nitrided layers increased with increasing nitriding temperature and time. Accordingly, a higher wear resistance was obtained.[23]

Investigation of the effect of PN parameters on the microstructure of SG cast iron is important for optimizing wear resistance in various industrial applications. Response Surface Methodology (RSM) is one of the methods used for the optimization of SG cast iron parameters.[24,25] In a study, the cutting parameters of GGG40 using wire electrical discharge machining technology and the surface roughness and process time of the cut surfaces were investigated. Optimization of the cutting parameters; table feed rate pulse time and pulse space were performed with RSM. The table feed rate was found to be the most effective parameter on the surface roughness and process time.[24] In another study, the optimization of the laser cladding process parameters used in the cladding of GG25 with iron powder was investigated with RSM. The laser power, scanning speed and powder feeding rate were used as the optimization input parameters. The effect of input parameters on the clad layer width, clad layer height, substrate melting depth and dilution rate was investigated and optimized.[25] The effect and optimization of plasma nitriding parameters on the microstructure of SG cast iron is a subject that needs to be investigated. This study aims to investigate the effect of plasma nitriding process parameters on the wear of GGG60, an SG cast iron, and to optimize these parameters according to wear performance.

Material and Method

Sample Preparation

In this study, friction disks were produced according to DIN EN 1563 GGG60, a pearlitic grade of SG cast iron. Two cylindrical wooden molds, 400 mm in length and 50 mm in diameter, were produced for casting. The wooden molds were prepared for sand casting. The casting process was carried out in a 500 kg capacity, medium frequency, 450 kW electric induction furnace without preheating. Pig iron of 130 kg, scrap steel of 140 kg, copper of 4 kg, silicon of 6 kg, Fe–Si–Mg of 3.5 kg, carbon of 5.5 kg and 0.5 kg 75Fe–Si post inoculant were

melted to 1410 °C. The melted alloy was poured into the crucible mold. After the part cooled down, it was removed from the mold and the residues on the surfaces were cleaned by sandblasting. The riser and runner were separated from the casting, thus producing the cast bars. The stages of the casting process are shown in Figure 1. The bars were CNC machined into disks with a diameter of 49.5 mm and a thickness of 5 mm. The chemical composition of samples of the disks was analyzed with an optical spectrometer. The chemical composition, tensile strength and elongation of GGG60 are shown in Table 1.

Plasma Nitriding (PN) Process

Plasma Nitriding (PN) is the treatment of gas atoms by ionization through heat, radiation or electrical discharge. For PN, atomic-sized nitrogen is supplied to the surface of the workpiece in a controlled vacuum environment. High voltage electrical energy accelerates the nitrogen atoms and thus plasma is formed. The resulting ion bombardment heats the workpiece, cleans its surfaces and provides nitriding. The parameters affecting PN can be listed as process gas mixture, nitriding temperature, nitriding time and plasma power.[26] PN process Figure 2 in detail. In this study, nitriding temperature and nitriding time were investigated comparatively.

In this study, PN was carried out with a bell-type plasma nitriding furnace. PN processes were carried out under 500 mbar vacuum pressure in a 70% H_2-30% N_2 environment. The processes were applied at three different temperatures and for three different process durations. Details of the process parameters are shown in Table 2. At the end of each process, the samples were control cooled to room temperature in the PN furnace.

Wear Tests

Wear tests were performed under dry wear conditions with a ball-on-disc tribometer. The wear test device is also capable of instantaneously calculating and monitoring the coefficient of friction (COF). The friction balls used in the experiments were 6 mm in diameter and made of tungsten carbide (WC). The duration of the experiments was 60 minutes, the frequency was 40 Hz and the sliding speed was 8 mm/s. The experiments were performed at three different loads for each PN condition and wear traces were created on the same sample at 3 mm distance.



Figure 1. Casting process.

Table 1. Chemical Composition of GGG60 (%) and Tensile Strength

C	Si	Mn	P	S	Cr	Cu	Mg	Fe	Tensile strength (MPa)	Elongation (%)
3.80	2.52	0.291	0.035	0.007	0.01	0.53	0.043	Balanced	620	3

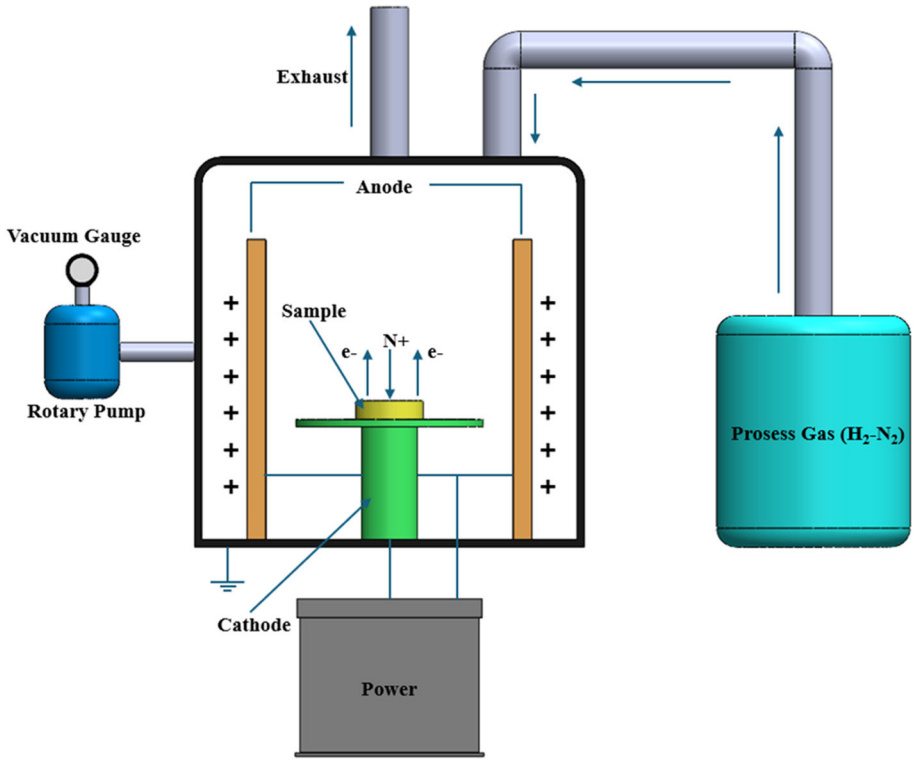

Figure 2. Plasma nitriding process.

Table 2. Plasma Nitriding Parameters

PN Parameter									
Temperature (°C)	400	400	400	450	450	450	500	500	500
Treatment duration (h)	0.5	2	4	0.5	2	4	0.5	2	4
Sample code	A1	A2	A3	B1	B2	B3	C1	C2	C3

Table 3. WC Ball Specification and Experimental Details

WC ball specification	Load (N)	Sliding speed (mm/s)	Frequency (Hz)	Test duration (min)
Diameter: Ø6 mm	10	8	40	60
Standard: ISO 3290 G10	20	8	40	60
Hardness: 1800 HV_{10}	30	8	40	60

Experimental details and the properties of the WC ball are given in Table 3. The schematic representation of the test mechanism is shown in Figure 3.

For microstructural characterizations, specimens were cut from the cross section with a diamond saw and mounted in bakelite. Specimens were ground with 60–1000 quality SiC abrasive papers and then polished with 3 µm diamond paste, respectively. All specimens were cleaned with ethanol and then dried. The microhardness changes along the cross-section was measured using a Vickers pyramid type microhardness tester (Metkon brand DUROLINE-M Vickers hardness device). Measurements were taken at 50 µm spacing, with a load of 200 g and 15 seconds dwell time. After hardness measurements, the specimens were ground again, polished with a 3 µm diamond solution. Etched with 3% nital solution, cleaned with ethanol and dried. Microstructural changes along the cross-section and wear surfaces were investigated by SEM (MAIA3 model produced by TESCAN) and EDS analysis.

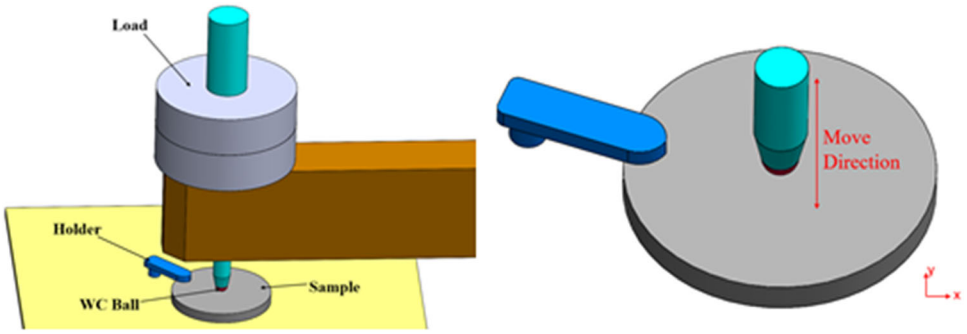

Figure 3. Schematic representation of wear test mechanism.

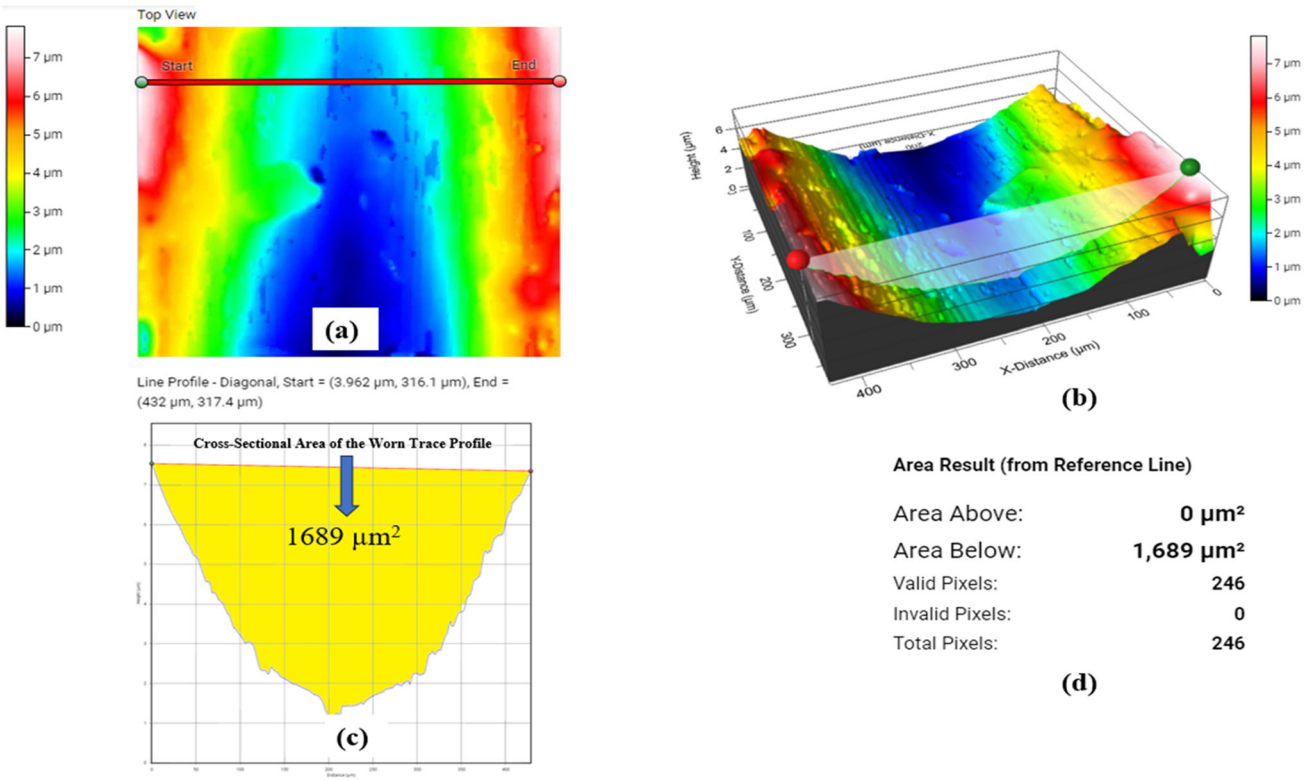

Figure 4. 2D surface profile (a), 3D surface profile (b), profile of cross-sectional area of the worn trace (c) and cross-sectional area of the worn trace (d) of sample B1 worn with 30 N normal load.

In analyzing the wear pattern and the wear volume, 2D wear profiles were created using a 3D surface profilometer (Filmetrics). Using the software of the profilometer, the wear track area of the wear track depth and width was automatically calculated. The wear volume was found by multiplying the wear track length by the wear track area as expressed in Eqn. 1. The wear track length is constant for each wear track at 6 mm. The sliding distance is also constant for each wear track at 28.8 m. Volume loss for each sample type and normal load was calculated by averaging 3 different wear zones on the track. Specific wear rates were calculated using Eqn. 2:[27]

$$V = AL \qquad \text{Eqn. 1}$$

where; V is the worn volume (m^3), A is cross-sectional area of the worn trace (m^2), L is the worn trace length (m).

$$w = \frac{V}{FS} \qquad \text{Eqn. 2}$$

where; w is spesific wear rate, V is the worn volume (m^3), S is the sliding distance (m), and F is the applied normal load (N).

The 2D surface profile (a), 3D surface profile (b), profile of the cross-sectional area of the worn trace (c) and cross-sectional area of the worn trace (d) of the B1 specimen subjected to 30N normal load generated by the profilometer are shown in Figure 4.

Statistical Analysis and Optimization

Surface hardness and hardness depth are affected by nitriding temperature and duration.[21] It is also important to analyze the changes in wear mechanisms and wear volume concerning loading variations. Experimentally investigating and analyzing in detail for all parameters is almost impossible in terms of time and cost. For these reasons, various statistical methods and modeling have been developed to determine the optimum conditions. One of the most effective of these methods is Response Surface Methodology (RSM). RSM optimizes the input parameters and output parameters to generate predictions that are very close to reality.[28] In this study, there are three independent inputs: temperature (°C), treatment duration (h) and wear load. The outputs are volume loss and specific wear rate. The optimization aims to determine the conditions where the volume loss and specific wear rate are the lowest. Thus, it will be possible to determine the best wear strength for parts made of GGG60 with PN applied. The experimental design for RSM was designed using the MiniTab software program. In RSM, the input parameters are specified as in Eqn. 3; [29]

$$y = F(x_1, x_2, x_3, \ldots, x_m) \quad \text{Eqn. 3}$$

where $x_1, x_2, x_3, \ldots, x_m$ and y represent input and output variables, respectively. The basic principle of RSM is to correlate inputs with outputs. This is achieved by modeling a quadratic equation (Eqn. 4);[29]

$$y = b_0 + \sum_{i=1}^{m} b_i x_i + \sum_{i=1}^{m-1} \sum_{j \geq i}^{m} b_{ij} x_i x_j + \sum_{i=1}^{m} b_{ii} x_i^2 + \varepsilon \quad \text{Eqn. 4}$$

In the equation, i represents the linear coefficient, j represents the second order coefficient, b represents the regression coefficient, m represents the number of parameters, and ε represents the error identified in the response. Three-factor Box-Behnken experimental design was used in the study and 15 tests were selected in accordance with the design. A Normality test was used to examine the distribution of the results and Box-Cox analysis was performed for non-normally distributed results. In addition, the effect ratios of the parameters were determined by Analysis of Variance (ANOVA). All statistical procedures were performed for 95% confidence interval.

Result and Discussion

Microstructure Analysis

The microstructure of the untreated sample was analyzed according to ASTM E2567-11 standard using Imagej Software. Microstructure and phases are shown in Figure 5. Here the graphite nodules are colored blue, the ferrite phase is grey and the pearlite phase is green. According to the results, ferrite phase was found around the graphite nodules. The ferrite phase was surrounded by the lamellar pearlite phase. The microstructure was as expected and following the literature.[30] The area of graphite particles was calculated using Eqn. 5 according to "maximum ferrite diameter (MFD)", which refers to the largest diameter of graphite nodule. Shape factor (SF) was found using Eqn. 6.[31] The nodularity of the graphite particles was found by ratios of the areas with the reference perfect circle of the same diameter (Eqn. 7). This process was repeated for three graphite particles in different regions and averaged. The ratios of ferrite, pearlite and graphite in the microstructure and the number of graphite per mm^2 were calculated with Imagej Software, which has been proven accurate for the analysis of ductile cast iron in many studies.[32,33] The microstructural analysis of the untreated sample is given in Table 4.

$$Area\ of\ Reference\ Circle = \frac{\pi(Maximum\ Ferrite\ Diameter)^2}{4} \quad \text{Eqn. 5}$$

$$Shape\ Factor(SF) = \frac{Area\ of\ Graphite\ Particles}{Area\ of\ Reference\ Circle} \quad \text{Eqn. 6}$$

$$Nodularity\ of\ Graphite(\%) = SF \times 100 \quad \text{Eqn. 7}$$

By applying PN to the samples, the compound layer, diffusion zone and core layer which nitride atoms cannot reach are formed from outside to inside respectively. It is known that the diffusion depth obtained after the PN process increases with increasing temperature and process duration.[34–36] Increasing the nitriding depth also increases the microhardness along the cross-section and affects the wear performance.[37] When the sections were investigated by SEM, there was a darker compound layer on the surface, a diffusion zone below it. SEM and EDS results (Figure 6) show that the depth of the nitriding affected zone of the sample A2; treated with 2 h PN at 400 °C (a) was 5 µm, sample C2; treated with 2 h PN at 500 °C (b) was 8 µm and sample C3 treated with 4 h PN at 500 °C (c) was 10 µm. Nitrogen diffusion rate increases with increasing temperature. The results obtained indicate that the thickness of both the compound layer and the diffusion zone increases with the increase in temperature and PN duration. Dalcin et al. applied PN to DIN 18MnCrSiMo6-4 specimens and found that increasing PN duration increases the thickness of the compound layer and diffusion zone for equal temperatures and PN environment.[38] Similarly, it has

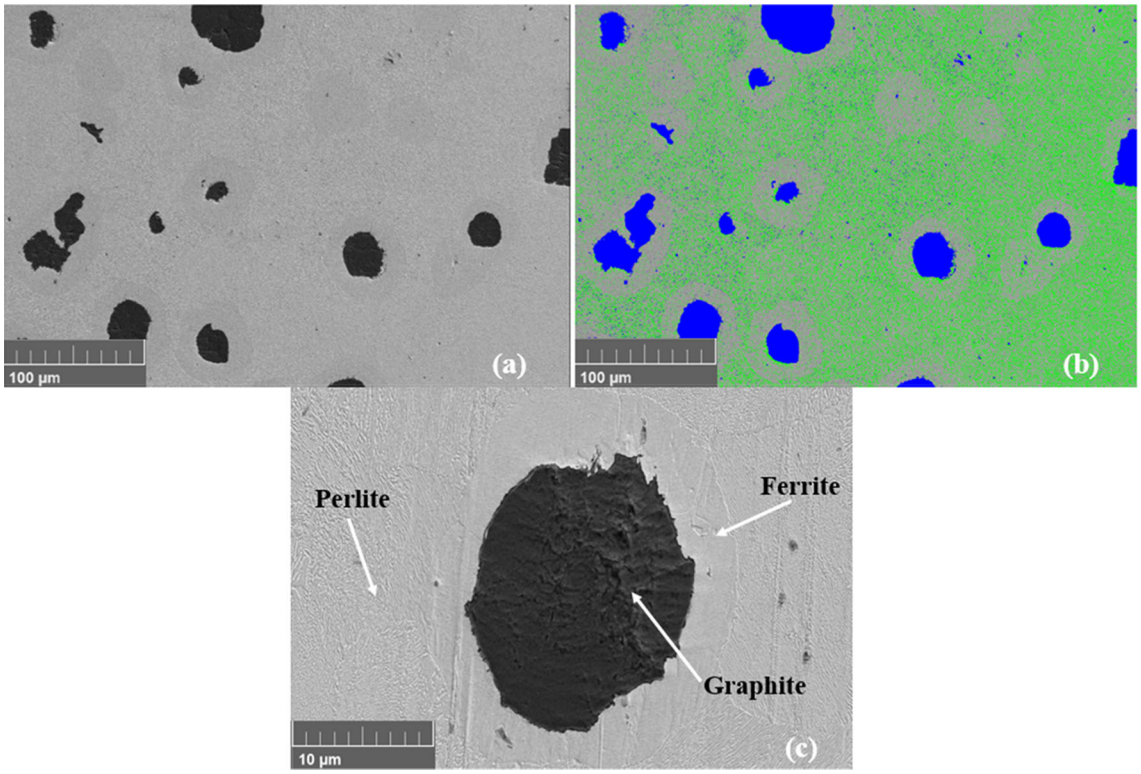

Figure 5. SEM of untreated sample (a), Imagej pattern (b) and microstructural details (c).

Table 4. Microstructural Analysis Results of the Untreated Sample

Specification	Value
Ferrite (%)	25.11
Pearlite (%)	60.63
Graphite (%)	14.26
Average graphite diameter (µm)	38.77
Nodularity of graphite (%)	88.14
Graphite (quantity/mm^2)	141

been proven in various studies that raising the processing temperature increases both the thickness of the compound layer and the diffusion zone.[36,39–41]

When the microhardness results (Figure 7a) are analyzed, the maximum hardness was obtained in the sample C3 with 592 $HV_{0.2}$. The minimum hardness was found in the untreated sample (235 $HV_{0.2}$). The hardness of the PN treated specimens increased to between 100 and 300 µm. This indicates the deepest region that the diffusion zone can reach. When the results are analyzed, hardness values increase with the increase in temperature and PN duration. It has been proven in various studies that hardness increases with the rise of both temperature and PN duration.[34,37,38,41] Riazi et al. in their investigations on 17-4 PH stainless steel found that PN increased both core hardness and surface hardness. They also proved that increasing both temperature and PN duration increased the hardness by a large amount.[34] Likewise, Liu et al. found that the increase in processing time for each condition increased the hardness of the SG cast iron specimens treated with QPQ (Quench-Polish-Quench), a nitrocarburizing method.[36] In another study, it was observed that the hardness values of AISI 4140 specimens treated with 1–4 h PN between 400 and 600 °C increased with rising temperature and treatment duration.[37]

The compound layer depth was also increased with increasing both temperature and PN duration, as shown in Figure 7b. It was observed that the penetration depth affected by the process also increased in parallel with the increase in compound layer depth. Thus, the increase in temperature and PN duration increased the compound layer depth, diffusion zone and hence the penetration depth. The penetration depth of 250 µm was obtained in the sample C3 with 4 h PN at 500 °C, while this penetration depth was 150 µm in the sample A1. While the compound layer depth was 2 µm in A1, this value increased up to 10 µm in C3. Similarly, Unal et al. applied PN to AISI 304 and found that the penetration depth increased with rising temperature and duration.[21] Similarly, SG cast iron showed a significant increase in hardness and penetration depth at higher nitriding temperatures.[23]

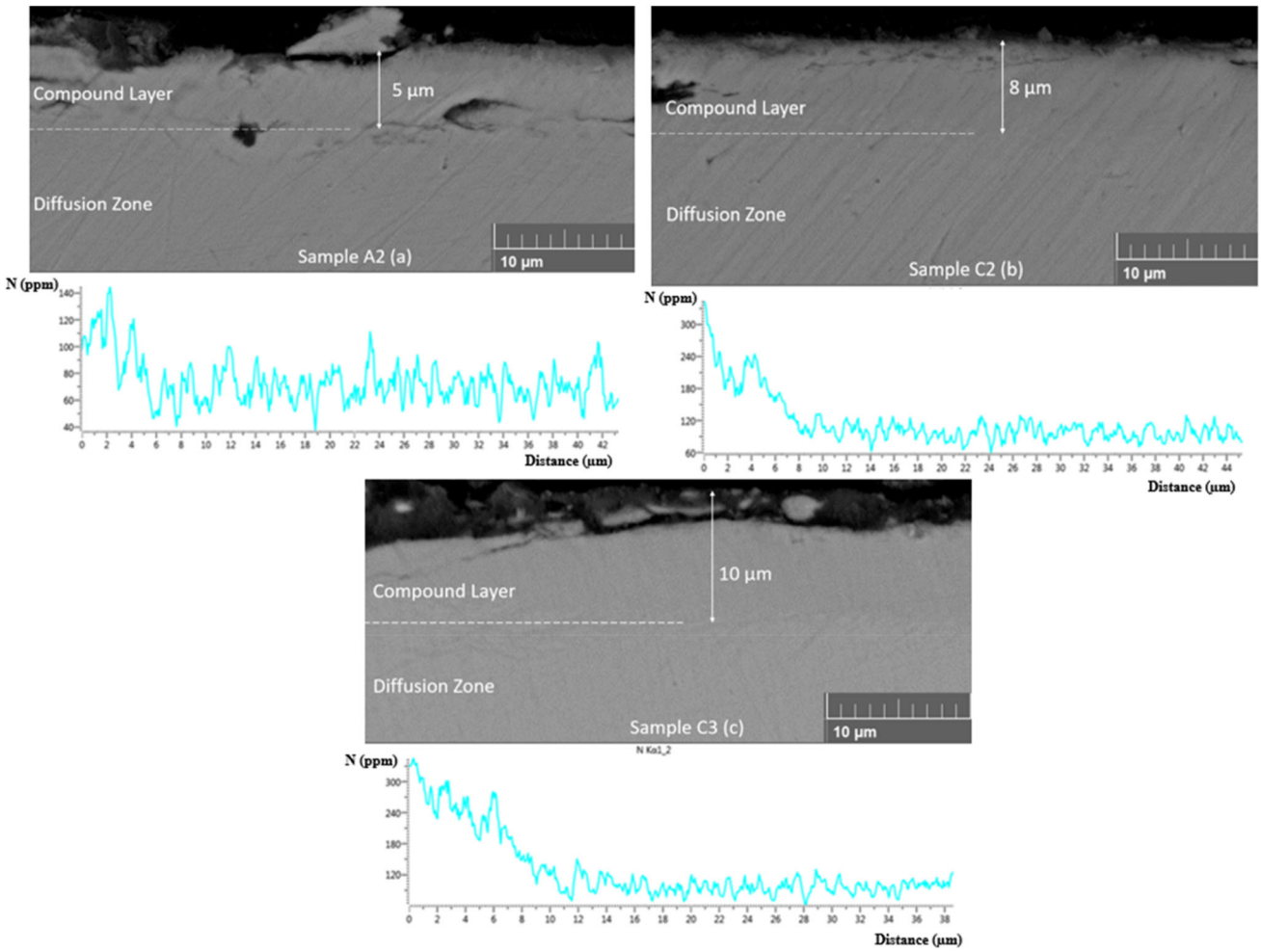

Figure 6. Results of samples A2 (a), C2 (b) and C3 (c) cross sectional area of SEM and EDS.

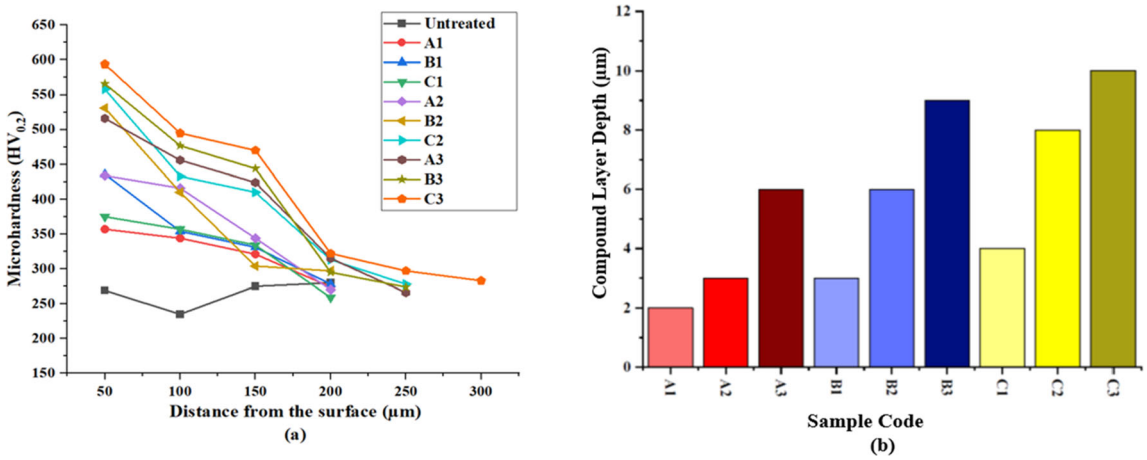

Figure 7. Change of a the microhardness according to distance from the surface and b the compound layer thickness according to sample code.

Friction and Wear Behavior

When the coefficient of friction (COF) results (Figure 8) were analyzed, it was determined that PN increased COF in general. The best COF was obtained in the untreated sample with an average of 0.055, while the worst COF was obtained in samples C2 and C3. This can be explained by the nitrided layer deposited on the surface which

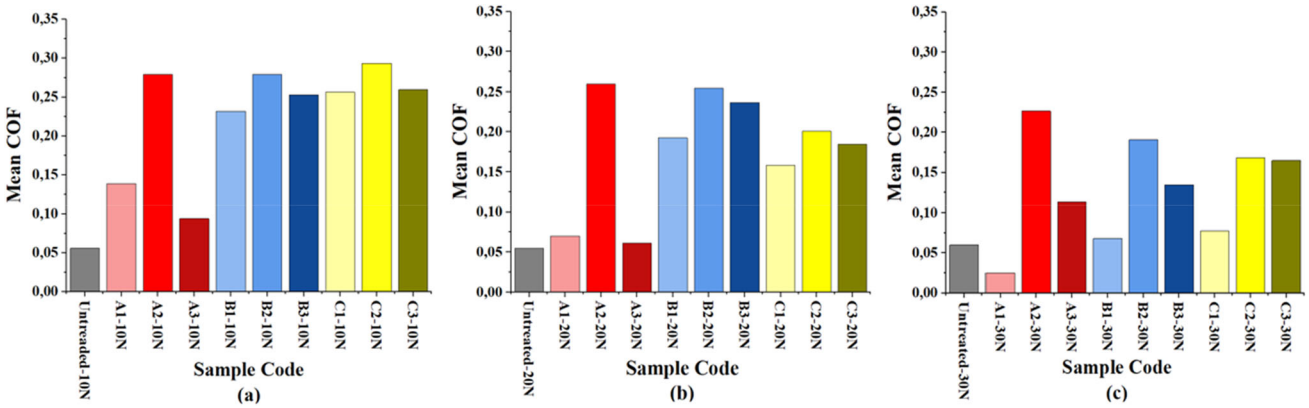

Figure 8. Mean friction coefficients according to PN parameters for (a) untreated and PN-treated wear load 10 N, (b) untreated and PN-treated wear load 20 N, and (c) untreated and PN-treated wear load 30 N.

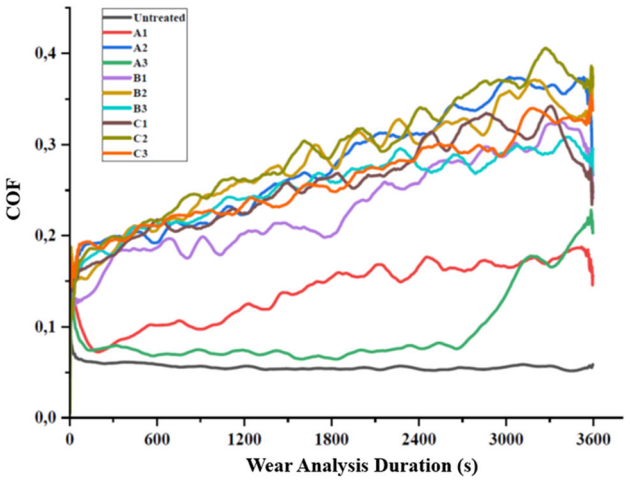

Figure 9. Friction coefficients change under 10 N load.

deteriorates the surface quality.[42] In general, it was observed that COF decreased with increased wear load. This is due to the increase in the plastic deformation, the increase in the wear load and the roughness on the worn surfaces is smoothed and a lower coefficient of friction is obtained. Figure 9, shows that the COF increased with increasing wear duration. This can be explained by the acceleration of wear with increasing wear duration, widening of the wear track and increasing the contact surface.[43]

It is known that an increase in surface hardness increases wear resistance. However, brittleness also increases with the increase in hardness. In addition, the increase in hardness also reduces the wear surface area.[43] Figure 10 shows that the width of the wear track is greatest in the untreated sample. It was also found that the wear behavior was commonly in the form of plastic deformation. At the same time, delamination was observed. In the PN treated specimens, the wear track width and deformation decreased due to the increase in hardness. Wear cracks and deformation were concentrated around the graphite (Figure 10c). The graphite nodules were broken in some areas and the deformation increased around these spaces. In the untreated sample with 10 N wear load, it was observed that wear microcracks were formed and these microcracks merged and formed delamination. In 20 N and 30 N loads, it was observed that the delamination area increased with the increase in load. In the PN treated specimen, microcrack formation was limited at 10 N loading (Figure 10d), the beginning of delamination was observed at 20 N loading (Figure 10e), and partial delamination was observed at 30 N loading (Figure 10f). It was also observed that microcrack formation increased around the delamination. Delamination wear was more common in PN treated specimens. The wear width decreased due to the effect of the tough layer formed by PN on the surface. The decrease in the wear width means a decrease in the contact surface. With the decrease in the contact surface, the contact surface pressure exerted by the friction ball on the wear surface increased relatively. With the increase in contact surface pressure, delamination also increases. In addition, the increase in hardness also leads to an increase in brittleness. Kara et al. stated in their research on cold work tool steels that the increase in contact surface pressure and hardness-related brittleness increases delamination.[43]

The volume loss (Figure 11) analysis showed that the most worn specimens for each condition were untreated sample independent of the loading condition. The wear resistance of the PN-treated specimens improved with the increase in the loading condition. This is related to the increase in surface hardness.[44,45] For all specimens PN treated at 400 °C, the volume loss gradually decreased with increasing treatment duration. This can be explained by the fact that the layer thickness affected by nitriding increases with process duration. The increase in layer thickness creates a harder internal structure. This also increases wear resistance. It was found that the sample B1 also suffered similar volume loss as the B1. This is due to the fact that the compound layer and diffusion zone on the B1 is similar to B1. The friction ball easily worn the compound layer and diffusion zone for both samples and reached the core

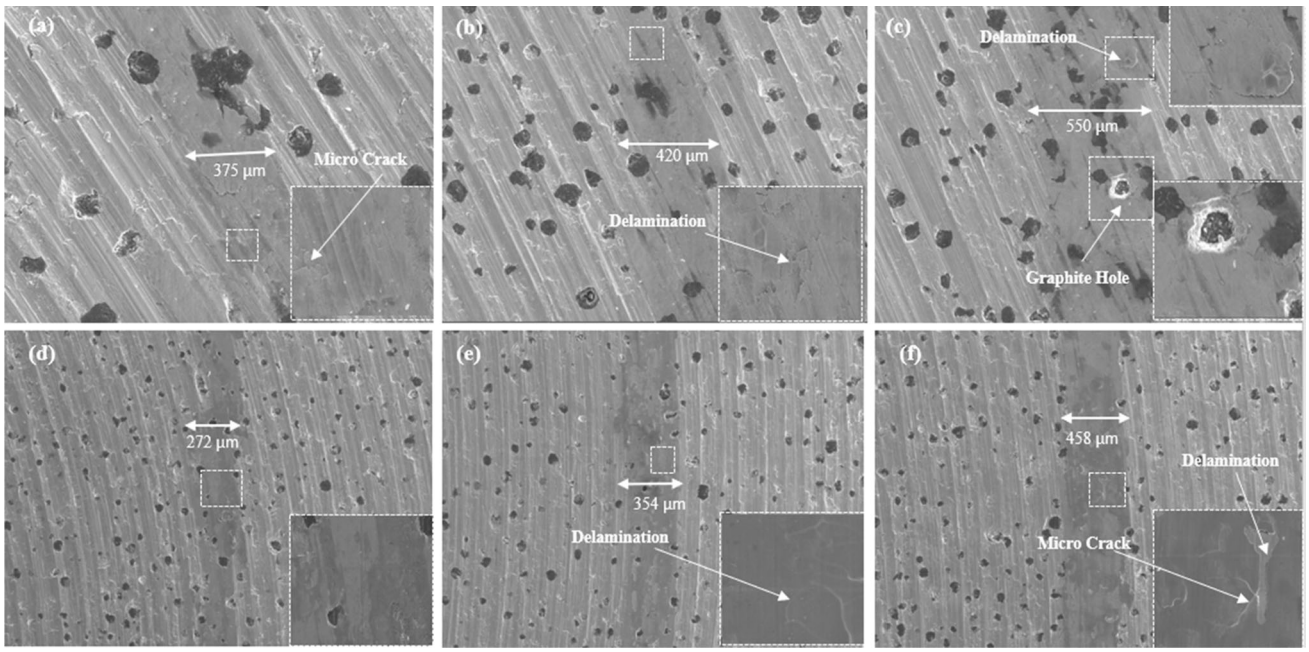

Figure 10. SEM of the wear track Untreated-10 N (a), Untreated-20 N (b), Untreated-30 N (c), B3-10 N (d), B3-20 N (e), B3-30 N (f).

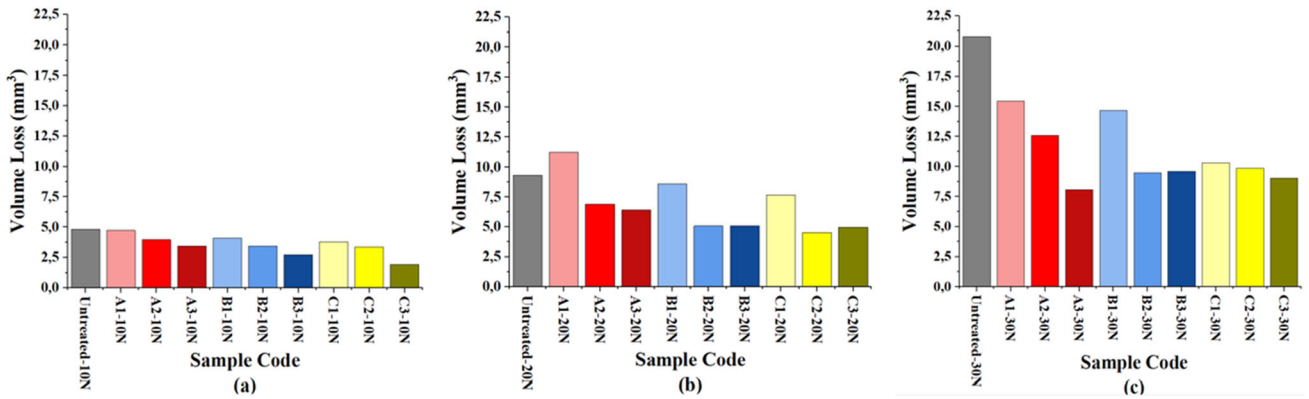

Figure 11. Volume loss (mm^3) according to PN parameters for (a) untreated and PN-treated wear load 10 N, (b) untreated and PN-treated wear load 20 N, and (c) untreated and PN-treated wear load 30 N.

zone. In the C1 sample, a thicker compound layer and diffusion zone were created with the effect of temperature increase. It was observed that the wear losses of the 4 h PN treated samples and the B2 and C3 samples were similar to each other. This is related to the fact that the wear cannot reach the core region with the increase in the thickness of the compound layer and diffusion zone. When the results are analyzed in general, volume loss decreases with the increase in both temperature and process duration. The results also show parallels with the hardness results. Ali et al. compared the wear performance of Ti-6Al-4V specimens with and without PN treatment and found that PN improved the wear performance by reducing the volume loss. In addition, it was also stated that the increase in PN duration improves the wear performance by decreasing the volume loss and increasing the hardness.[46] As the wear load increases, the volume loss increases for all conditions. This is related to the increase in contact surface pressure due to the increase in normal force.[39]

Specific wear rate (WR) results (Figure 12) showed that the specimens with the highest wear rate were untreated specimens. In the 30 min PN treated specimens, the WR was found to be lower than the untreated specimens although higher than the other specimens. This is due to the fact that the very thin compound layer is easily worn away and the friction ball reaches the less hard sublayers more easily. When the specimens with PN applied at equal times were examined, it was determined that the increase in temperature decreased the WR. This is due to the increase in the thickness of the compound layer and the diffusion zone with rising temperature. These harder zones made the

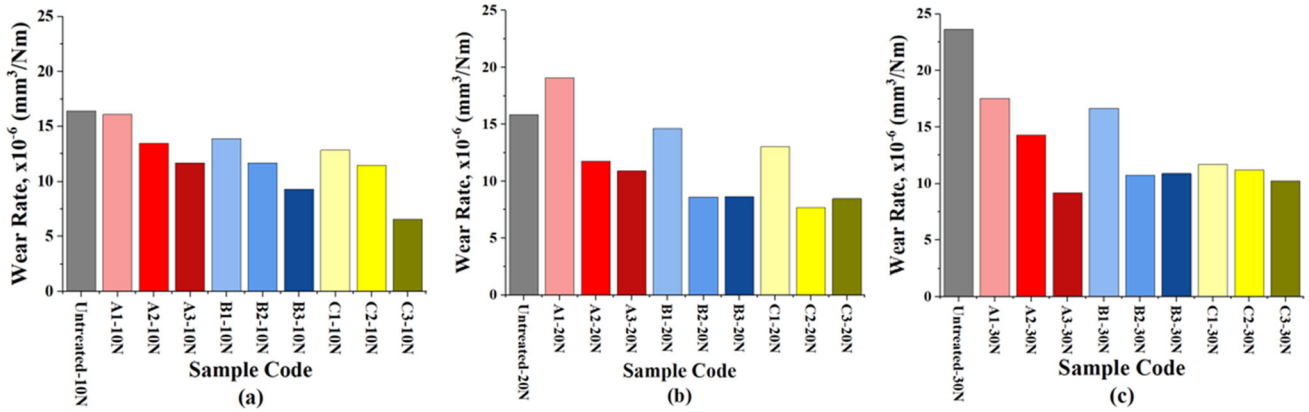

Figure 12. Specific wear rate (%) according to PN parameters for (a) untreated and PN-treated wear load 10 N, (b) untreated and PN-treated wear load 20 N, and (c) untreated and PN-treated wear load 30 N.

Table 5. The Design Matrix and Experimental Response Variable Values Were Used to Evaluate the Wear Process

Test no	A	B	C	Temperature (°C)	Treatment duration (h)	Wear load (N)	Volume loss (mm^3)	Wear rate [(10^{-6} mm^3)/Nm]
1	− 1	0	− 1	400	2	10	3.948	13.45
2	0	0	0	450	2	20	5.0646	8.63
3	0	− 1	1	450	0,5	30	14.664	16.65
4	0	0	0	450	2	20	5.0646	8.63
5	− 1	− 1	0	400	0,5	20	11.214	19.10
6	1	− 1	0	500	0,5	20	7.662	13.05
7	0	− 1	− 1	450	0,5	10	4.0746	13.88
8	0	1	− 1	450	4	10	2.7312	9.30
9	− 1	0	1	400	2	30	12.582	14.29
10	1	0	1	500	2	30	9.876	11.21
11	0	0	0	450	2	20	5.0646	8.63
12	− 1	1	0	400	4	20	6.408	10.91
13	0	1	1	450	4	30	9.6	10.90
14	1	1	0	500	4	20	4.968	8.46
15	1	0	− 1	500	2	10	3.3672	11.47

wear more difficult and decreased the WR. In the PN treated samples at the same temperature, it was found that the increase in PN duration decreased the WR. The main reason for this situation is again the increase in the hardened layer thickness due to the nitriding effect and the difficulty of wear. When both temperature and PN duration are high, the WR results for the same loading conditions are close to each other. This is related to the fact that the wear depth remains within the hardened zone and cannot reach the core. When the WR results are analyzed in general, it is seen that the decrease in WR varies in parallel with the set of the surface and sublayers. This is consistent with previous studies.[47,48]

Optimization

The optimization process was carried out to determine the effect of PN temperature (°C), process duration (h) and wear load (N) variation on volume loss (mm^3) and WR [(10^{-6} mm^3)/Nm] ratios. The experimental design and variables used in the optimization process are given in Table 5. The effect ratios and significance of the variables were analyzed by ANOVA. Values less than the 95% ($p > 0.05$) confidence interval were considered as non-significant. In RSM modeling, the p value must be less than 0.05 for a factor to be considered effective in the model.[28,49] As a result of the regression analysis, Box-Cox transformation was performed for volume loss since the true scale (λ=1) value was outside the upper and lower limits. For wear rate, no transformation was needed since

Table 6. ANOVA Results for Volume Loss and Wear Rate

		Volume loss				Wear rate			
	DF	Seq SS	Contribution (%)	*F* value	*P* value	Seq SS	F value	Contribution (%)	*P* Value
Model	9	186.371	99.12	62.73	0.000	136.444	16.38	96.72	0.003
Linear	3	163.143	86.77	161.16	0.000	86.470	32.68	61.29	0.001
A-temperature	1	8.567	4.46	23.98	0.004	22.960	22.87	16.28	0.005
B-treatment duration	1	21.723	11.55	73.24	0.000	60.448	72.05	42.85	0.000
C-wear load	1	132.853	70.66	386.25	0.000	3.062	3.11	2.17	0.138
Square	3	17.99	9.57	18.17	0.004	46.695	16.82	33.10	0.005
A^2	1	2.874	1.53	13.22	0.015	11.702	17.39	8.29	0.009
B^2	1	8.957	4.76	30.52	0.003	21.799	26.29	15.45	0.004
C^2	1	6.159	3.28	18.66	0.008	13.195	14.25	9.35	0.013
2-way interaction	3	5.237	2.79	5.29	0.052	3.279	1.18	2.32	0.405
A*B	1	0.98	0.52	2.97	0.145	2.778	3.00	1.97	0.144
A*C	1	1.129	0,60	3.42	0.124	0.299	0.32	0.21	0.594
B*C	1	3.128	1.66	9.48	0.028	0.202	0.22	0.14	0.660
Error	5	1.65	0.88	–	–	4.628	–	3.28	–
Total	14	188.022	100	–	–	141.073	–	100	–

λ=1 was within the upper and lower limits. The *p* and *F* values of the model are given in Table 6. When Table 6 is examined, it is seen that PN temperature, process duration and wear load value are effective in modeling. The parameter that affects volume lost the most is wear load with 70.66% according to RSM modeling results. The increase in wear load increased the contact pressure, the increase in pressure increased the plastic deformation and accelerated the wear. The effect of temperature on volume loss was 11.55% while the effect of PN process duration on volume loss was 4.46%. The most effective parameter on wear rate was found to be treatment duration at 42.85%. The effect of temperature on WR was 16.28% and the effect of wear load was 2.17%.

The R^2 values of the model (Table 7) are 99.12% for volume loss and 96.72% for wear rate. The predictive ability of the model (Adj. R^2) was calculated as 85.96% for volume loss and 47.31% for wear rate. The volume loss prediction equation generated by RSM is shown in Eqn. 8 and the WR prediction equation is given in Eqn. 9.

$$Volume\ Loss = 97,9 - 0,403^{*}A - 5,01^{*}B + 0,476^{*}C + 0,000435^{*}A^2 + 0,553^{*}B^2 + 0,01292^{*}C^2 + 0,00563^{*}A^{*}B - 0,001063^{*}A^{*}C - 0,0503^{*}B^{*}C \quad \text{Eqn. 8}$$

$$Wear\ Rate = 210,5 - 0,795^{*}A - 9,53^{*}B - 0,421^{*}C + 0,000835^{*}A^2 + 0,860^{*}B^2 + 0,01890^{*}C^2 + 0,00948^{*}A^{*}B - 0,000547^{*}A^{*}C - 0,0128^{*}B^{*}C \quad \text{Eqn. 9}$$

Using Eqn. 8, the volume loss of the previously measured sample C3 under 30 N normal load was calculated as 9.21 mm^3. The value found by experimental methods as a result of measurements for the sample in question is 9.024 mm^3. In this case, the model can predict the result with a small error of 2.11%. The wear rate of specimen sample C3 under 30 N normal load was calculated as 10.246 (10^{-6} mm^3)/Nm. The value found by experimental methods for the same conditions is 11.1836 (10^{-6} mm^3)/Nm. The error rate for WR is 9.14. The predictions from the model and the values found by experimental methods are very close to each other. This proves that a robust model has been created and thanks to this modeling, the best results can be obtained with a small number of experiments, which is the main purpose of optimization with RSM.

Table 7. Model Summary

	S	R^2 (%)	Adj. R^2 (%)	Pred. R^2 (%)
Volume loss (mm^3)	0.5745	99.12	97.54	85.96
Wear rate [(10^{-6} mm^3)/Nm]	0.9621	96.72	90.81	47.31

When the optimization results were examined (Table 8), it was seen that the least volume loss was obtained under a normal load of 10 N for specimens with 2.66 h PN applied at 459 °C. The decrease in volume loss with decreasing normal load was a natural result of the decrease in contact pressure. The decrease in contact pressure also minimizes the wear effect. In particular, the PN duration remained at

Table 8. Optimization Result

	Temperature (°C)	Treatment duration (h)	Wear load (N)
Volume loss optimum values	459	2.66	10
Volume loss optimum values for 10 N wear load conditions	459	2.66	10
Volume loss optimum values for 20 N wear load conditions	468	3.05	20
Volume loss optimum values for 30 N wear load conditions	478	3.47	30
Wear rate optimum values	465	3.12	18.89
Wear rate optimum values for 10 N wear load conditions	462	3.08	10
Wear rate optimum values for 20 N wear load conditions	465	3.12	20
Wear rate optimum values for 30 N wear load conditions	468	3.19	30

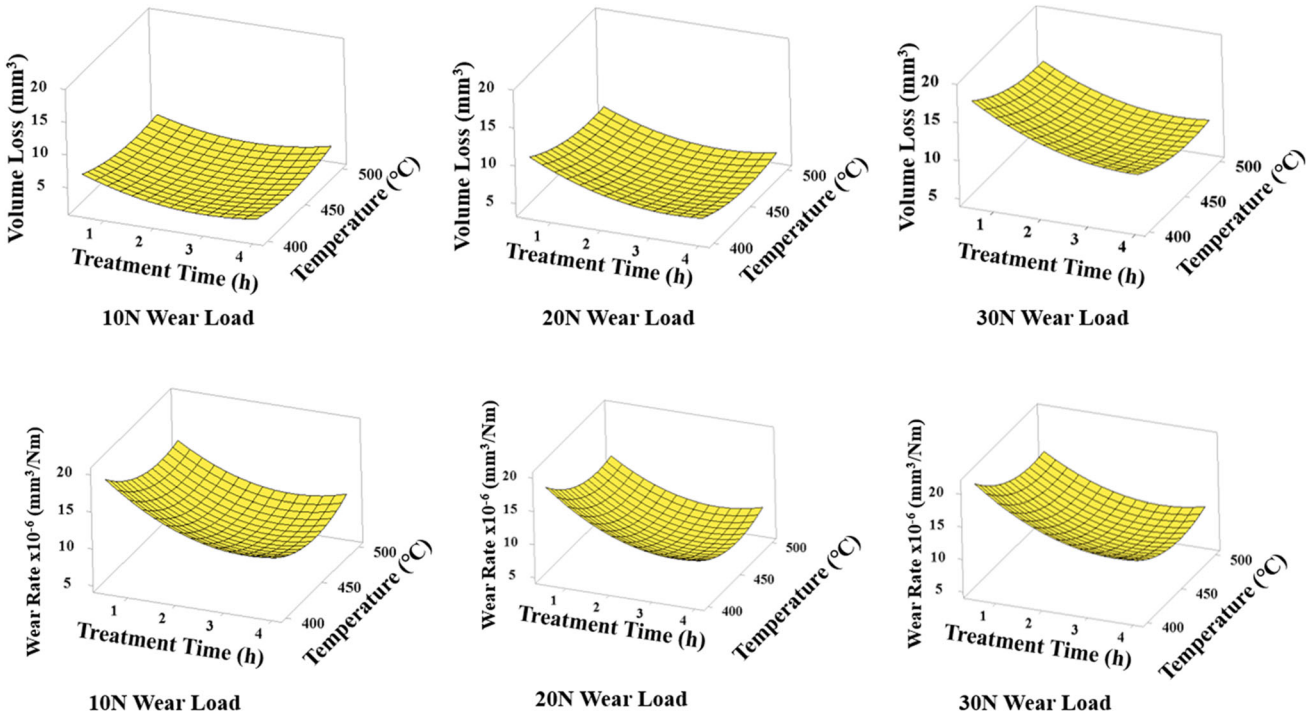

Figure 13. 3D Surface plot of RSM optimization results.

2.66 h, indicating that the ball under a wear load of 10 N could not abrade the nitriding and hardening layers and could not reach the core. When the wear load increased to 20 N, the minimum volume loss reached 468 °C and 3.05 h. This can be explained by the deepening and acceleration of wear with increasing wear load. When the wear load was increased by 30 N, it was found that the least volume loss was observed in the sample with 3.47 h PN at 478 °C. This is again related to the increase in wear with increasing wear load. The increase of temperature and PN duration increases both hardness (Figure 7a) and nitriding depth (Figure 7b). This makes wear more difficult and results in smaller volume loss. When the results are analyzed, it is clearly seen that the PN duration increases more with higher load. This proves that the PN duration has a greater effect on volume loss. Optimization results and previous research also support this situation.[46,50] The optimization results of the minimum volume loss for each loading condition concerning temperature and PN duration are shown in Figure 13. According to the results of WR optimization (Table 8), the minimum WR was obtained under 18.89N normal load for PN applied samples for 3.12 h at 465 °C. For 10N wear load, the minimum WR was obtained at 462 °C and 3.02h. For 30N wear load, these values increased to 468 °C and 3.18 h. The results are shown in Figure 13 as a 3D surface plot. The values where the minimum WR is obtained with the increase in load are again increasing with the increase in temperature and PN duration in parallel with the volume loss, but these changes are limited than the volume loss changes. The reason for this is that the changes in volume loss and load are parallel.

When the changes of volume loss according to various wear loads were analyzed, it was observed that the effect of the change in temperature and treatment duration was limited for the 10 N. This can be explained by the fact that the nitrided layer could not be completely worn and the core layer could not be reached. The effect of temperature and treatment duration on volume loss increased with the increase in wear load. For 20 N and 30 N loadings, it was found that the increase in temperature and treatment duration dramatically decreased the volume loss. When the WR results were analyzed, an increase in temperature and treatment duration up to about 470 °C and 3 h decreased the WR regardless of the wear load. The reason for the small increase in WR for higher temperature and treatment duration can be explained as the increased friction force with the increase in COF increases the wear.

Conclusion

In this study, the changes in the wear behavior of GGG60 spheroidal graphite cast iron treated to plasma nitriding for various temperatures and treatment duration were investigated for different wear load conditions. According to the results obtained:

- Plasma nitriding improved the wear performance of GGG60 regardless of the process parameter.
- Increasing both temperature and plasma nitriding duration increases the surface hardness and nitriding depth. The change of plasma nitriding duration has a greater effect on hardness and nitriding depth than temperature.
- The volume loss due to wear was found to be higher in untreated samples than all the samples treated with PN. Similarly, in parallel with the hardness and nitriding depth results, volume loss decreases with increasing temperature and plasma nitriding time. Increasing the wear load increased the volume loss. Wear rate results are also in parallel with volume loss.
- A model was created with Response Surface Methodology for volume loss and wear rate optimization. The R^2 values of the model are 99.12% for volume loss and 96.72% for wear rate. The prediction ability of the model (Adj. R^2) was calculated as 85.96% for volume loss and 47.31% for wear rate. The model was able to predict the sample C3 with an error of 2.11% for volume loss and 9.14% for wear rate with an error of 2.11% for volume loss and 9.14% for wear rate for the sample C3 with 30 N wear load, whose output values were previously calculated experimentally. The prediction results clearly show the success of the model.
- It was observed that the minimum volume loss was obtained under 10 N normal load for samples with 2.66 h PN at 459 °C. For WR, the minimum ratio was obtained under 18.89 N normal load for samples with 3.12 h PN applied at 465 °C.
- According to the optimization results, the most effective parameter on volume loss is wear load. Other effective parameters were found as process temperature and process duration, respectively. On the other hand, the most effective parameter on wear rate is process duration.

Acknowledgements

This work was supported by the Karabük University Scientific Research Projects Coordination Unit. Project Number: KBÜBAP-23-YL-037. The support is gratefully acknowledged.

Funding

Open access funding provided by the Scientific and Technological Research Council of Türkiye (TÜBITAK).

Open Access

This article is licensed under a Creative Commons Attribution 4.0 International License, which permits use, sharing, adaptation, distribution and reproduction in any medium or format, as long as you give appropriate credit to the original author(s) and the source, provide a link to the Creative Commons licence, and indicate if changes were made. The images or other third party material in this article are included in the article's Creative Commons licence, unless indicated otherwise in a credit line to the material. If material is not included in the article's Creative Commons licence and your intended use is not permitted by statutory regulation or exceeds the permitted use, you will need to obtain permission directly from the copyright holder. To view a copy of this licence, visit http://creativecommons.org/licenses/by/4.0/.

REFERENCES

1. F.D. de Oliveira, C.T.M. Anflor, J.N.V. Goulart, B. Baranoğlu, Nodular cast iron GGG40, 60, 70 mechanical characterization from bars and blocks obtained from brazilian foundry. Metals **12**, 1115 (2022). https://doi.org/10.3390/met12071115
2. A. Mourujärvi, K. Widell, T. Saukkonen, H. Hänninen, Influence of chunky graphite on mechanical and fatigue properties of heavy-section cast iron. Fatigue Fract. Eng. Mater. Struct. **32**, 379–390 (2009). https://doi.org/10.1111/j.1460-2695.2009.01337.x
3. S.C. Lin, T.-S. Lui, L.-H. Chen, J.-M. Song, Effect of pearlite on the vibration-fracture behavior of spheroidal graphite cast irons under resonant conditions.

Metall. Mater. Trans. A **33A**, 2623–2634 (2002). https://doi.org/10.1007/s11661-002-0384-y
4. P.R. Gangasani, Evaluation of fatigue strengths of continuously cast ductile irons. Int. J. Met. **1**, 41–55 (2007). https://doi.org/10.1007/BF03355417
5. K. Zhan, Y. Zhang, L. Bao, Z. Yang, B. Zhao, V. Ji, Surface characteristic and wear resistance of QT-700-2 nodular cast iron after laser quenching combing with shot peening treatment. Surf. Coat. Technol. **423**, 127589 (2021). https://doi.org/10.1016/j.surfcoat.2021.127589
6. D. Zhang, Z. Li, H. Fan, H. Rui, F. Gao, Microstructure and tribological properties of Fe-based laser cladding layer on nodular cast iron for surface remanufacturing. Coatings **11**, 974 (2021). https://doi.org/10.3390/coatings11080974
7. F.-J. Cárcel-Carrasco, M. Pascual-Guillamón, F. Salas-Vicente, V. Donderis-Quiles, Influence of heat treatment in the microstructure of a joint of nodular graphite cast iron when using the tungsten inert gas welding process with perlitic grey cast iron rods as filler material. Metals **9**, 48 (2019). https://doi.org/10.3390/met9010048
8. Y. Zhou, R. Liu, Z. Lao, S. Luo, Y. You, S. Sun et al., Enhancing cutting performance of Ti (C, N)-based cermet tools on nodular cast iron by incorporating high-entropy carbide. J. Am. Ceram. Soc. **106**, 6987–6994 (2023). https://doi.org/10.1111/jace.19314
9. C. Zhang, X. Shen, J. Wang, C. Xu, J. He, X. Bai, Improving surface properties of Fe-based laser cladding coating deposited on a carbon steel by heat assisted ultrasonic burnishing. J. Mater. Res. Technol. **12**, 100–116 (2021). https://doi.org/10.1016/j.jmrt.2021.02.076
10. G. Gumienny, A. Macioł, P. Macioł, Predicting the microstructure of compacted graphite iron using a fuzzy knowledge-based system. Arch. Civ. Mech. Eng. **23**, 87 (2023). https://doi.org/10.1007/s43452-023-00620-y
11. M. Górny, G. Angella, E. Tyrała, M. Kawalec, S. Paź, A. Kmita, Role of austenitization temperature on structure homogeneity and transformation kinetics in austempered ductile iron. Met. Mater. Int. **25**, 956–965 (2019). https://doi.org/10.1007/s12540-019-00245-y
12. E.L. Castellanos-Leal, D.A. Miranda, A.E. Coy, J.G. Barrero, J.A. González, O.P.V. Rueda, Induction hardening treatment and simulation for a grey cast iron used in engine cylinder liners. J. Phys. Conf. Ser. **786**, 12013 (2017). https://doi.org/10.1088/1742-6596/786/1/012013
13. S. Inthidech, K. Boonmak, P. Sricharoenchai, N. Sasaguri, Y. Matsubara, Effect of repeated tempering on hardness and retained austenite of high chromium cast iron containing molybdenum. Mater. Trans. **51**, 1264–1271 (2010). https://doi.org/10.2320/matertrans.M2010018
14. S. Inthidech, P. Sricharoenchai, Y. Matsubara, Effect of alloying elements on heat treatment behavior of hypoeutectic high chromium cast iron. Mater. Trans. **47**, 72–81 (2006). https://doi.org/10.2320/matertrans.47.72
15. S. Inthidech, P. Sricharoenchai, Y. Matsubara, Effect of molybdenum content on subcritical heat treatment behaviour of hypoeutectic 16 and 26 wt% chromium cast irons. Int. J. Cast Met. Res. **25**, 257–263 (2012). https://doi.org/10.1179/1743133612Y.0000000009
16. K.C. Chen, M.H. Hon, The urea nitrocarburizing of cast irons with various graphite morphologies. J. Mater. Sci. **24**, 2833–2838 (1989). https://doi.org/10.1007/BF02385634
17. E. Kondakci, N. Solak, The effect of microstructure on nitriding mechanism of cast iron. Int. J. Met. **14**, 1033–1040 (2020). https://doi.org/10.1007/s40962-019-00404-2
18. S.C. Serino, L. Bartlett, Nitriding of lightweight high manganese and aluminum steels. Int. J. Met. **9**, 78–81 (2015). https://doi.org/10.1007/BF03355607
19. M.S. Aghareb Parast, M. Jamalkhani Khameneh, M. Azadi, M. Azadi, M.H. Mahdipanah, S. Roostaie, Effect of plasma nitriding on high-cycle fatigue properties and fracture behaviors of GJS700 nodular cast iron under cyclic bending loading. Fatigue Fract. Eng. Mater. Struct. **44**, 2070–2086 (2021). https://doi.org/10.1111/ffe.13479
20. T. Nobuki, M. Hatate, Y. Kawasaki, A. Ikuta, N. Hamasaka, Effects of nitriding and nitro-carburizing on the fatigue properties of ductile cast iron. Int. J. Met. **11**, 52–60 (2017). https://doi.org/10.1007/s40962-016-0088-5
21. O. Unal, E. Maleki, R. Varol, Comprehensive analysis of pulsed plasma nitriding preconditions on the fatigue behavior of AISI 304 austenitic stainless steel. Int. J. Miner. Metall. Mater. **28**, 657–664 (2021). https://doi.org/10.1007/s12613-020-2097-x
22. T. Kumar, P. Jambulingam, M. Gopal, A. Rajadurai, Surface hardening of AISI 304, 316, 304L and 316L ss using cyanide free salt bath nitriding process, in *International Symposium of Research Students on Materials Science and Engineering,* (Chennai, 2004), pp. 1–11
23. Y. Hoshiyama, K. Chiba, T. Maruoka, Effect of active screen plasma nitriding on mechanical properties of spheroidal graphite cast iron. Metals **11**, 412 (2021). https://doi.org/10.3390/met11030412
24. K. Aydın, U. Levent, S. Güvercin, G.Ü.L. Ferhat, Investigation of the machining performance of ferritic ductile cast iron in WEDM using response surface methodology. Sigma. J. Eng. Nat. Sci. **40**, 95–107 (2022). https://doi.org/10.14744/sigma.2022.00008
25. R. Guo, Y. Zhao, L.J. Cui, Y. Cui, X.L. Li, B. ZhenG et al., Using response surface methodology (RSM) to optimize the key laser processing parameters for laser cladding of grey cast iron. Lasers Eng. **51**, 75 (2021)

26. Aghajani H, Behrangi S Plasma nitriding of steels, 1st edn., (Springer, Heidelberg, 2017), https://doi.org/10.1007/978-3-319-43068-3
27. Y. Küçük, E. Altaş, M.E. Topcu, A comparative analysis of the effect of laser surface treatment on the dry sliding wear behavior of ductile cast irons with different microstructures. Optik **274**, 170540 (2023). https://doi.org/10.1016/j.ijleo.2023.170540
28. A. Temiz, The effects of process parameters on tensile characteristics and printing time for masked stereolithography components, analyzed using the response surface method. J. Mater. Eng. Perform. (2023). https://doi.org/10.1007/s11665-023-08617-7
29. K. Wang, F. Lam, Quadratic RSM models of processing parameters for three-layer oriented flakeboards. Wood Fiber Sci. 173–86 (1999)
30. I. Mitelea, I. Bordeaşu, M. Pelle, C. Crəciunescu, Ultrasonic cavitation erosion of nodular cast iron with ferrite-pearlite microstructure. Ultrason. Sonochem. **23**, 385–390 (2015). https://doi.org/10.1016/j.ultsonch.2014.11.001
31. P. Prakash, V.D. Mytri, P.S. Hiremath, Digital microstructure analysis system for testing and quantifying the ductile cast iron. Int. J. Comput. Appl. **19**, 22–27 (2011). https://doi.org/10.5120/2342-3062
32. S. Toraman, T. Cosgun, B. Alkan, B. Çetin, O. Akyildiz, Assessing the volume fractions of the phases, nodularity and nodule count of spheroidal graphite cast ıron using ımagej software. Mugla J. Sci. Technol. **5**, 137–142 (2019). https://doi.org/10.22531/muglajsci.521128
33. N. Costa, N. Machado, F.S. Silva, A new method for prediction of nodular cast iron fatigue limit. Int. J. Fatigue **32**, 988–995 (2010). https://doi.org/10.1016/j.ijfatigue.2009.11.005
34. H. Riazi, F. Ashrafizadeh, S.R. Hosseini, R. Ghomashchi, Influence of simultaneous aging and plasma nitriding on fatigue performance of 17–4 PH stainless steel. Mater. Sci. Eng. A **703**, 262–269 (2017). https://doi.org/10.1016/j.msea.2017.07.070
35. S.M.Y. Soleimani, A.R. Mashreghi, S.S. Ghasemi, M. Moshrefifar, The effect of plasma nitriding on the fatigue behavior of DIN 1.2210 cold work tool steel. Mater. Des. **35**, 87–92 (2012). https://doi.org/10.1016/j.matdes.2011.09.067
36. Y. Liu, Y. Sun, W. Zhang, X. Du, Effect of QPQ nitriding parameters on properties of pearlite ductile cast iron. Int. J. Met. **14**, 556–563 (2020). https://doi.org/10.1007/s40962-019-00384-3
37. H. Kovacı, Ö. Baran, A.F. Yetim, Y.B. Bozkurt, L. Kara, A. Çelik, The friction and wear performance of DLC coatings deposited on plasma nitrided AISI 4140 steel by magnetron sputtering under air and vacuum conditions. Surf. Coatings Technol. **349**, 969–979 (2018). https://doi.org/10.1016/j.surfcoat.2018.05.084
38. R.L. Dalcin, L.F. Oliveira, I.L. Diehl, V.W. Dias, A.D.S. Rocha, Response of a DIN 18MnCrSiMo6-4 continuous cooling bainitic steel to plasma nitriding with a nitrogen rich gas composition. Mater. Res. (2020). https://doi.org/10.1590/1980-5373-mr-2020-0036
39. Q. Wang, C. Huang, L. Zhang, Microstructure and tribological properties of plasma nitriding cast CoCrMo alloy. J. Mater. Sci. Technol. **28**, 60–66 (2012). https://doi.org/10.1016/S1005-0302(12)60024-3
40. Q. Wang, L. Zhang, H. Shen, Microstructure analysis of plasma nitrided cast/forged CoCrMo alloys. Surf. Coatings Technol. **205**, 2654–2660 (2010). https://doi.org/10.1016/j.surfcoat.2010.10.031
41. Y. Li, Y. He, J. Xiu, W. Wang, Y. Zhu, B. Hu, Wear and corrosion properties of AISI 420 martensitic stainless steel treated by active screen plasma nitriding. Surf. Coatings Technol. **329**, 184–192 (2017). https://doi.org/10.1016/j.surfcoat.2017.09.021
42. J. Kang, M. Wang, W. Yue, Z. Fu, L. Zhu, D. She et al., Tribological behavior of titanium alloy treated by nitriding and surface texturing composite technology. Materials **12**, 301 (2019). https://doi.org/10.3390/ma12020301
43. F. Kara, Y. Küçük, O. Özbek, N.A. Özbek, M.S. Gök, E. Altaş et al., Effect of cryogenic treatment on wear behavior of Sleipner cold work tool steel. Tribol. Int. **180**, 108301 (2023). https://doi.org/10.1016/j.triboint.2023.108301
44. H. Mindivan, Effects of combined diffusion treatments on the wear behaviour of hardox 400 steel. Procedia. Eng. **68**, 710–715 (2013). https://doi.org/10.1016/j.proeng.2013.12.243
45. X. Nie, L. Wang, Z.C. Yao, L. Zhang, F. Cheng, Sliding wear behaviour of electrolytic plasma nitrided cast iron and steel. Surf. Coatings Technol. **200**, 1745–1750 (2005). https://doi.org/10.1016/j.surfcoat.2005.08.046
46. M. Mubarak Ali, S. Ganesh Sundara Raman, S.D. Pathak, R. Gnanamoorthy, Fretting wear behaviour of plasma nitrided Ti-6Al-4V fretted against unnitrided Ti-6Al-4V and alumina counterbodies. Trans. Indian Inst. Met. **62**, 59–64 (2009). https://doi.org/10.1007/s12666-009-0008-y
47. E. Feldshtein, O. Devojno, S. Wojciechowski, M. Kardapolava, I. Kasiakova, On the microstructure, microhardnessand wear behavior of gray cast iron surface layer after laser strengthening. Materials **15**, 1075 (2022). https://doi.org/10.3390/ma15031075
48. J.O. Agunsoye, S.A. Bello, I.O. Awe, A.A. Yekinni, R.G. Adeyemo, A.O. Ologunagba, Effects of graphite additions and heat treatment on the microstructure, mechanical and tribological properties of 13% chromium white iron. J. Miner. Mater. Charact. Eng. **2**, 270 (2014). https://doi.org/10.4236/jmmce.2014.24032
49. S. Simsek, S. Uslu, Determination of a diesel engine operating parameters powered with canola, safflower

and waste vegetable oil based biodiesel combination using response surface methodology (RSM). Fuel **270**, 117496 (2020). https://doi.org/10.1016/j.fuel.2020.117496

50. D. She, S. Liu, J. Kang, W. Yue, L. Zhu, C. Wang et al., Abrasive wear resistance of plasma-nitrided Ti enhanced by ultrasonic surface rolling processing pre-treatment. Materials **12**, 3260 (2019). https://doi.org/10.3390/ma12193260

Publisher's Note Springer Nature remains neutral with regard to jurisdictional claims in published maps and institutional affiliations.